2018

High-resolution Infrared Spectroscopy of the v23 and v22 Vibrational Bands of Methyl Vinyl Ketone

Michael Iranpour
Connecticut College, michaeliranpour@gmail.com

High-resolution infrared spectroscopy of the v_{23} and v_{22} vibrational bands of methyl vinyl ketone

Michael Iranpour
Connecticut College
Department of Chemistry
May 3, 2018

Advisor: Jacob Stewart
Readers: Tanya Schneider, Stanton Ching

Table of Contents

"The scientist is not a person who gives the right answers, he is one who asks the right questions"

- *Levi Strauss*

"If you would be a real seeker after truth, it is necessary that at least once in your life you doubt, as far as possible, all things"

- *Rene Descartes*

1. Acknowledgements

First and foremost, I would like to extend the greatest thank you to my advisor Jacob Stewart. I still remember the day I walked into his office for the first time as a sophomore with little to no knowledge of physical chemistry, asking if I could work with him during the coming summer. Ever since that first summer, his guidance and seemingly endless patience continues to inspire me to keep learning. Jacob's enthusiasm for chemistry has made the time I've worked for him the most enjoyable of my academic career. Little did I know that the impromptu visit to his office my sophomore year would be such a pivotal moment that has since helped define my years at Connecticut College, and for that I am incredibly grateful.

I would also like to thank the other members of the Stewart lab who I have worked with over the years. To Minh, Tyler, Marcus, and Yiyan: thank you all for your continued support and friendship. Working with you has made the time spent in lab all the more enjoyable, especially when "the physical chemistry just wasn't working."

To my friends, the so-called "social scientists," thank you for your support in the classes we have shared, the times spent working in the Hale conference room where nights turned to mornings, and for making my experience at Connecticut College the best it could be.

Lastly, I would like to thank my parents for their unwavering support throughout the years. I owe all of my experiences at Connecticut College to them, for without them, none of this would have been possible.

2. Abstract

The high-resolution Infrared spectrum of methyl vinyl ketone (C_4H_6O) has been acquired in the region containing the v_{22} and v_{23} bands near 987 cm^{-1} and 1001cm^{-1}, respectively, using a quantum cascade laser-based spectrometer. All acquired spectra underwent frequency calibrations that will prove useful during future atmospheric measurements of methyl vinyl ketone. Anharmonic calculations were performed at the MP2/ccp-pVTZ level of theory to obtain the vibrational frequencies and the excited state rotational constants of *cis*-methyl vinyl ketone. These calculations supported the assignment of the Q-branch features at 1001.031 and 987.592 cm^{-1} to the v_{22} and v_{23} fundamental vibrations of the molecule. Additionally, the Q-branch feature at 998.98 cm^{-1} was assigned as a hot band of the v_{23} mode arising from the v_{26} mode. The calculated rotational constants were used as starting points to begin preliminary spectral simulations of the v_{22} and v_{23} bands.

3. Introduction

3.1 Preliminary

Biogenic Volatile Organic Compounds (BVOCs) are naturally occurring organic molecules that play critical roles in atmospheric chemistry. BVOCs are emitted by vegetation, and processed within plant canopies, primarily contributing to tropospheric chemistry processes.[1] These compounds are generally highly reactive as their molecular structure is built upon isoprene units, giving rise to double bond and conjugated double bond systems. Due to their increased reactivity, BVOCs will react readily with many atmospheric species; some naturally occurring, such as molecular oxygen, and some anthropogenic, such as nitric oxides.[2] These reactions are just

two of the many atmospheric processes that demonstrate the environmental effects of BVOCs. The reactions with nitric oxides tend to form ozone, a primary constituent of smog, while the oxidation of BVOCs will lead to the formation of secondary organic aerosols.[3] Secondary organic aerosols are known as "processed BVOCs" and when condensed form the haze that is often observed in forest canopies. Aerosols help to defend against some biotic stresses by either absorbing or reflecting radiation, altering the immediate climate by warming, or cooling the area. Methyl vinyl ketone (MVK) is one of the most abundant BVOCs as it is the primary product resulting from both the photooxidation and ozonolysis of isoprene. MVK's high relative abundance is the result of isoprene's status as the most abundant BVOC, comprising approximately half of all BVOC emissions.[1,4] The structure of MVK can be seen in Figure 1.

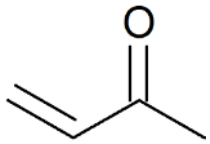

Figure 1: Structure of methyl vinyl ketone (C_4H_6O).

The environmental importance possessed by MVK and other BVOCs has necessitated the development of techniques to study them in atmospheric concentrations and conditions. The use of various spectroscopic techniques, specifically methods involving infrared (IR) spectroscopy, have been explored because not only is MVK IR active, but other atmospheric molecules such as water and carbon dioxide lack absorption bands in an IR window where MVK absorbs strongly.[5] Analyzing the IR spectra of atmospheric samples would be made incredibly difficult if the target region included molecules like water as the IR spectrum of water has regions that are heavily congested and would make identifying and distinguishing peaks from MVK, or other BVOCs

difficult. These factors influenced the decision to acquire a laser that could perform spectroscopic experiments with an IR range of 970 – 1019 cm^{-1}.

MVK has been studied using a plethora of instrumental methods including rotational[6] and Fourier transform IR spectroscopy[7], and gas chromatography[8]. These methods have been implemented to both perform concentration measurements, as well as analyze MVK's involvement in numerous atmospheric processes under variable environmental conditions.[9] One recent study of interest by Lindenmeier et al[5] performed gas-phase mid-IR, far-IR, and liquid Raman measurements of MVK, acquiring its entire IR spectrum. Additionally, the work done by Lindenmeier et al. included performing ab initio calculations at the B3LYP and MP2 levels of theory that resulted in the determination of the vibrational frequencies for each mode of both the *cis* and *trans* conformers of MVK. The ab initio calculations provided enough information for the complete assignment of the fundamental vibrational transitions in the IR spectrum.

Although previous works on MVK have successfully covered a wide range of spectral analysis, they are lacking in the acquisition of high-resolution spectra. In this study, previous works are expanded upon with the presentation of the rotationally resolved high-resolution spectrum of MVK in the region containing the ν_{23} and ν_{22} vibrational modes from 970-1015 cm^{-1}. The relatively high intensity with which these bands absorb coupled with the fact that atmospheric molecules such as water do not absorb in this range makes them reasonable targets when performing IR spectroscopy of MVK. Additional vibrational bands were also identified near the ν_{23} and ν_{22} modes. In order to begin the assignment of these additional vibrational bands, anharmonic vibrational frequencies as well as rotational constants were predicted at the MP2-ccpVTZ level of theory.[10] Although the anharmonic frequencies have been calculated previously, the calculation of the rotational constants was necessary for simulating the spectrum of MVK. In order to accurately

simulate the spectrum, minute adjustments to the calculated rotational constants are made in the simulation in the attempt to mimic the observed rotational spectrum.

3.2 Ro-vibrational Spectroscopy

Different regions of the electromagnetic spectrum are used to investigate various molecular processes. Typically, different regions of the electromagnetic spectrum are divided into sections that identify the types of molecular processes that may be studied using that type of radiation. The different ranges of the electromagnetic spectrum, along with the associated molecular processes that such radiation induces are included in Table 1, adapted from McQuarrie.[11]

Table 1: The regions of the magnetic spectrum and the molecular processes that are induced by that type of radiation.[11]

Region	Microwave	Far-IR	IR	Visible / ultraviolet
Wave number (cm^{-1})	0.033 - 3.3	3.3 - 330	330 – 14500	14500 - 50000
Molecular Process	Rotation of Polyatomic molecules	Rotational transitions of small molecules & low energy vibrations of large molecules	Vibrational transitions	Electronic transitions

In this work, IR spectroscopy was performed on MVK in the gas phase in order to observe the compound's vibrational transitions.

Although rotational transitions are not of particular interest when studying and identifying atmospheric processes and molecules, they accompany vibrational transitions. Rotational transitions are not normally resolved when performing vibrational spectroscopy, but the resolution achieved when using the quantum cascade laser manages to resolve the rotational structure quite well. The final type of transition, electronic, is not observed as higher energy radiation is required

to induce the transitions than what can be supplied with IR methods. An apt model for the vibrational transitions that are observed is the an/harmonic oscillator seen in Figure 2.

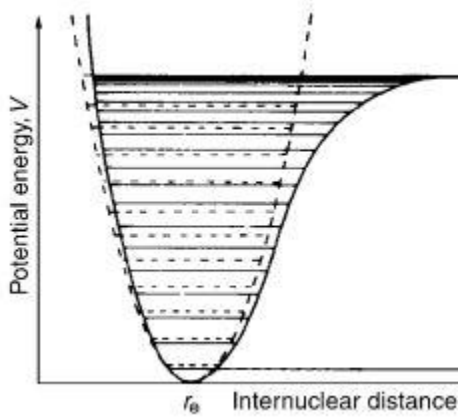

Figure 2: A harmonic oscillator (dashed curve) and an anharmonic oscillator (solid curve) are used to demonstrate the different vibrational levels of a single vibrational mode of a molecule.[12]

The anharmonic and harmonic oscillator both accomplish the same goal: identifying discrete vibrational levels of a molecule, and providing a model for calculating their energies. The difference between the two, is that the anharmonic oscillator manages to take into account factors that would help to increase the accuracy of the approximations assumed when using the models. For example, the anharmonic model takes into account the decrease in energy spacing between subsequent vibrational energy levels, as well as the fact that bonds can break. Both of these examples are pictured in the comparison of the two models in Figure 2. Rotational transitions are also excited by IR radiation and visible in high-resolution spectra acquired in the IR because the rotational levels are found in between the vibrational transitions. Unlike vibrations, each consecutive energy level is farther from its predecessor than the last. Rotational transitions are often modeled by the 'rigid rotor' in which the rotor can only spin at specific speeds designated by their energy level, J. This means that if a molecule undergoes a rotational transition from J = 0

→ J = 1, the change in angular momentum is instant. Instantaneous, discrete transitions are said to be quantized, meaning, in the case for a rotational motion, that it is impossible for the molecule to be rotating at speeds existing between the various rotational levels. This confines the energies of rotations to integer values of J so that J = 0, 1, 2, etc. A diagram of rotational energy levels for a diatomic molecule can be seen in Figure 3.

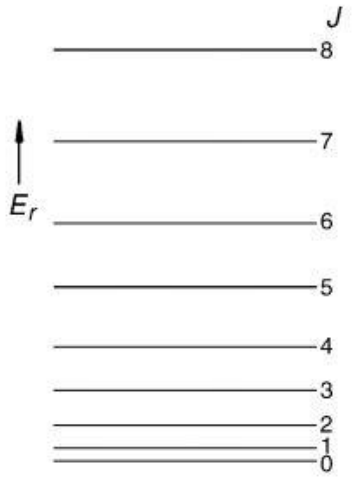

Figure 3: Rotational energy level diagram for a diatomic molecule showing relative energy differences between rotational levels (J).[12]

The changes in dipole moment experienced by molecules during vibrational transitions are associated with vibrational modes. A molecule's vibrational modes consist of all of the possible molecular vibrations that occur when the atoms within the molecule are moving in a periodic motion when both translational and rotational motion are constant. The number of vibrational modes a molecule can experience is given by Equation 1, where N is equal to the number of atoms in the molecule.[11] Using this equation, it is found that MVK has 27 vibrational modes.

$$3N - 6 \qquad (1)$$

Each vibrational mode has a vibration frequency, *v*, which corresponds to how much energy is required in order to excite that specific vibrational motion. Each vibrational motion can be treated as its own harmonic oscillator, with the energy of each vibrational level given by Equation 2 where h is Planck's constant, and E_v is the energy for the vibrational level. An important take away from this equation is that the difference in energy of the vibrational levels is equal to *v*.[11]

$$E_v = hv(v + \frac{1}{2}) \qquad (2)$$

The relationship between a mode's vibrational frequency and the energy required to excite that mode is defined by Equation 3, where E is the energy required to excite the vibration.[11]

$$E = hv \qquad (3)$$

These relationships allow the vibrations of MVK to be modeled as 27 independent harmonic oscillators, each with their own fundamental frequency of $v = 0 \rightarrow v = 1$.

Rotational transitions are similar in character to vibrational motion, but are the result of immediate changes of the angular momentum of a molecule. The energy of a diatomic molecule, which has one possible axis of rotation, is given by Equation 3, where J is the rotational energy level, and B is the rotational constant for the molecule. The rotational constant for an individual molecule is given by Equation 4, where c is the speed of light and I is the moment of inertia for a diatomic molecule.

$$E(J) = B * J(J+1) \qquad (3)$$

$$B = \frac{h}{8\pi^2 cI} \qquad (4)$$

Polyatomic molecules, such as MVK, can have three moments of inertia, one for each rotational axis. When an atom in a polyatomic molecule rotates at a fixed distance from its center of mass, it possesses three different angular velocities corresponding to the x, y, and z axes which all intersect at the molecule's center of mass. The introduction of rotations over three independent axes gives rise to a total of three rotational constants, a, b, and c; each with their own moment of inertia I_a, I_b, and I_c. Each rotational constant must now be considered when dealing with polyatomic molecules, and the equation for the constants A, B, and C, are given by Equations 4.1, 4.2, and 4.3.[11]

$$\mathrm{A} = \frac{h}{8\pi^2 cI_a} \qquad (4.1)$$

$$\mathrm{B} = \frac{h}{8\pi^2 cI_b} \qquad (4.2)$$

$$\mathrm{C} = \frac{h}{8\pi^2 cI_c} \qquad (4.3)$$

Molecules with three separate moments of inertia are known as asymmetric tops, and can be characterized by the magnitude of each of the rotational constants.

Rotational and vibrational transitions share the quality of being 'quantized,' meaning that there are discrete energy levels where the molecule is able to exist. These constraints are presented in the form of selection rules, which are essentially guidelines that dictate the types of transitions that may occur. The selection rules for the rotational transitions of a diatomic molecule, and molecular vibrations are as follows:

Vibrational selection Rules (harmonic oscillator)

* $\Delta v = \pm 1$,
* The dipole moment must vary during a molecule's vibration

Rotational Selection Rule for a rigid rotator (diatomic molecule)

* $\Delta J = \pm 1$

IR spectroscopy involves both rotational and vibrational transitions, where the different frequencies of light that are absorbed by the molecule are directly related to the differences in energy between vibrational and rotational energy levels. Due to the small differences in energy of rotational transitions, the spacing between individual rotational lines is generally very small and high-resolution spectroscopy is required to resolve separate rotational transition lines in an IR spectrum. In order to resolve the rotational spectrum using IR methods, it is necessary to have an instrument that is capable of high-resolution spectroscopy. The region of a molecule's spectrum that involves an excitation from the ground vibrational state to the first excited state without changes in *J* is called the Q-branch, and gives rise to an intense vibrational band. The transitions that not only involve a change in vibrational state, but also a change in *J* will generate rotational lines that are either higher, or lower in frequency than the Q-branch. The lines generated at a higher energy are the result of a $\Delta J + 1$ transition, while the lines generated at a lower energy are the result of $\Delta J - 1$ transitions.[11] The website spectraplot[13] is commonly used to model spectra of molecular absorbance using spectroscopic data acquired from the HITRAN[14] database. A spectrum of nitrous oxide was generated using spectraplot coupled with HITRAN data to demonstrate relative P-, Q-, and R- branch structures in Figure 4.

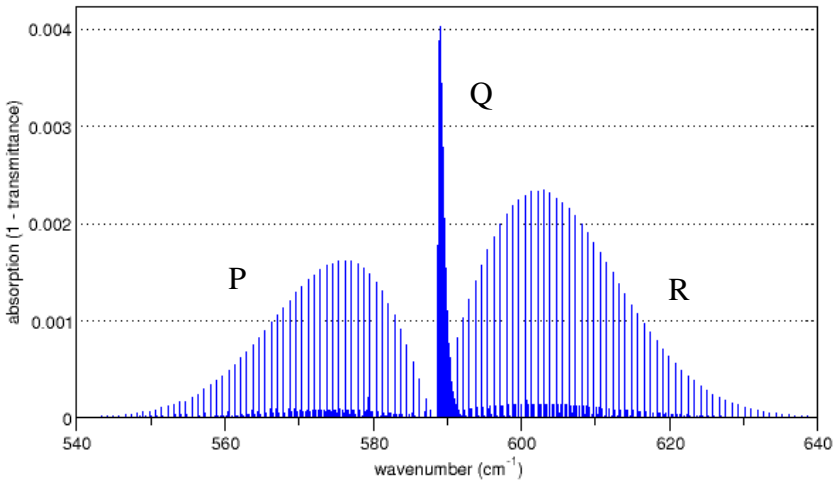

Figure 4: A simulated absorbance spectrum of nitrous oxide where the labeled P, Q, and R branches are easily identifiable.

3.3 Quantum Cascade Lasers

In this study, it was imperative that the spectrometer be capable of acquiring high-resolution spectra. Having the ability to acquire rotationally resolved spectra facilitates both the assignment of the observed transitions, and will assist with analyzing atmospheric samples in the future by making it easier to differentiate MVK from other molecules. Furthermore, it was essential that the laser for the spectrometer have an adjustable tuning range so that varying ranges of spectra could be acquired. These requirements lead to the acquisition of a quantum cascade laser (QCL) for use in the spectrometer.

QCLs are semiconductor lasers that emit in the mid- to far-infrared range of the electromagnetic spectrum.[15] Unlike most gas lasers that require pumping in order to connect discrete energy levels so that photons are released upon electron relaxation, semiconductor lasers emit photons upon the recombination of electron-hole pairs across a band gap. In semiconductors,

electrons are able to occupy two different energy bands: the conduction and valence band. The valence band exists at a lower energy than the conduction band, populated by a greater majority of the electrons in the material, while the conduction band is populated by a smaller proportion of the electrons in the material.[11] In a semiconducting material, there is a separation in energy between the two bands called the band gap. The band gap is essentially an energy range in a solid where no electronic states exist for the electrons to populate. Electrons existing in the conduction band that relax down to the valence band will emit a single photon with a wavelength that is equal to that of the band gap. This is the process by which most semiconductor lasers function. The function by which QCLs are driven is different than that of a standard semiconductor laser in that the electrons undergo what are known as intersubband transitions.[16] In the case of a QCL, an intersubband transition is the excitation or relaxation of an electron from one quantized electronic energy level within the conduction band to another within the same band. The electron never fully relaxes to the valence band. QCLs are constructed as a series of layers, varying in thickness that exist at decreasing energies according to the voltage that is applied across the QCL material. The layers in the QCL structure are more commonly known as quantum wells. Quantum wells are essentially potential wells that each have a discrete energy value and in the case of QCLs, are constructed with a thickness on the order of the de Broglie wavelength of the electrons. When in these quantum wells, the electrons are confined to only a single dimension of movement and require the application of a voltage to traverse the energy gap to the next quantum well that exists at a lower energy. It is the relaxation of an electron within a well that emits a photon. The electron will then tunnel to the next well where it will relax again, releasing another photon. The efficiency of QCLs comes from the fact that a single electron does emit a single photon. The electron relaxes in one well which releases a photon before tunneling to the next well where this process is repeated.

This allows for a single electron to produce many more photons than the single photon emitted from the relaxation of an electron from the conduction band to the valence band in a standard semiconductor. A diagram of the movement of an electron through a QCLs lasing medium is presented in Figure 5.

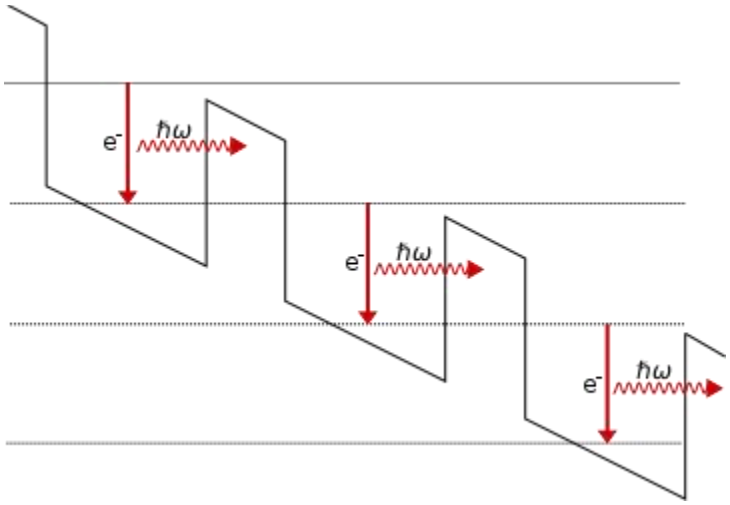

Figure 5*:* Transition diagram of an electron as it tunnels through wells, emitting a photon with each instance of relaxation.[17]

The type of QCL used for this study is called an "external cavity"-QCL. Normally, the wavelength of light emitted by a QCL is fixed by the lasing material, but the inclusion of an external cavity allows for the selection of a range of wavelengths that the laser can produce. The high optical power output, tuning range, and ability to operate at room temperature make the use of QCLs an optimal method when performing research involving high-resolution infrared spectroscopy ranging from the analysis of breath samples to characterizing gas phase processes in the atmosphere.[18,19]

4. Experimental

4.1 QCL Spectrometer

A quantum cascade laser (QCL)-based spectrometer was constructed to perform high-resolution infrared spectroscopy on the BVOC methyl vinyl ketone. The light source for the spectrometer is a mode-hop free external cavity QCL that was purchased from Daylight Solutions. The QCL has a tunable range of 962-1019 cm^{-1} with a linewidth of ~0.0018 cm^{-1}. The beam is split with a ZnSe beam-splitter (ThorLabs, BSW710). Half of the light passes through a reference cell (CRD Optics, 0.5 m Sample Cell 903-0001) that contains pure methanol at a pressure of less than 1 torr. The light is then collected by photovoltaic MCT detector (Vigo systems, PVM-10.6-1x1) that is run at room temperature. The other half of the light is sent through a multipass absorption cell (Aerodyne Research, AMAC-76), that contains a sample of methyl vinyl ketone. The beam path is coordinated in such a way that it enters the multipass cell at a 3.2º angle so that the highly reflective mirrors on either side of the multipass cell may send the beam back and forth inside the cell for a theoretical path length of 76 m. The light exiting the cell is then directed to a thermoelectrically cooled MCT detector (Vigo Systems, PVI-2Te10.6-1x1). The electrical signals from the two detectors are digitized by a data acquisition card (Labjack, U6) and saved on the lab computer. A simple diagram of the spectrometer is presented in Figure 6.

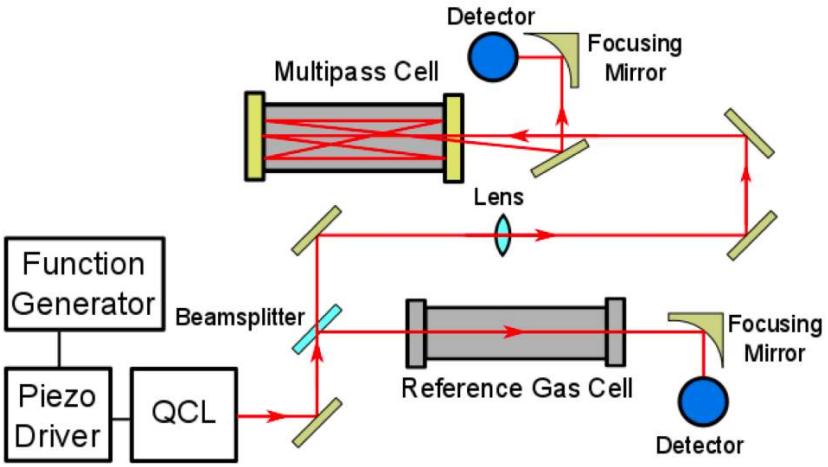

Figure 6 Diagram of the QCL-based spectrometer[20]

Two different scanning methods were used to acquire spectra of methyl vinyl ketone. The first scanning method used was a 'sweep scan.' The QCL is fitted with a mechanical motor, which allows for the laser to sweep across a designated wavelength range by altering the angle of a diffraction grating within the laser. Preliminary sweep scans were used to rapidly acquire broader ranges of the Infrared spectrum, providing an overall picture of the vibrational bands and rotational structure. Although useful for acquiring an overview of the spectrum, performing a sweep scan has its faults when considering high-resolution spectroscopy. Sweep scans are prone to mode hops, peak distortion, and error in the frequencies of the spectra. A piezo scanning method was implemented to overcome these issues. A piezo scan requires a function generator (Siglent, SDG1025) as well as the piezo controller (Thorlabs, MDT694B). The piezo controller only scans a small wavenumber range, ~0.7cm^{-1} with a sine function created by the function generator. The function generator was set to a frequency of 3 Hz, amplitude of 10 Vpp and an offset of 5Vdc. The piezo scanning method is made possible as the QCL is equipped with a piezoelectric material with a mirror on it. A piezoelectric material is a solid that has the ability to change in size when a voltage is applied. When the function generator applies the voltage sinusoidaly, the piezoelectric material

in the laser is constantly fluctuating in size, altering the wavelength of the emitted light. Signal to noise is improved greatly when performing piezo driven scans as the spectrometer scans over the same area many times, allowing for signal averaging. The piezo scans also have a higher reproducibility from scan to scan, while sweep scans can contain peak distortions and mode hops. Although the piezo scanning method improves upon many of the issues experienced with the sweep-scan method, it is limited by the fact that only ~0.7 cm^{-1} of spectra can be acquired per scan. In order to construct a spectrum that includes the entire target range of the spectrum, several dozen spectra must be acquired and subsequently calibrated. When performing piezo scans, a new sample must be prepared for every acquisition as the multipass cell must be evacuated in between acquisitions in order to acquire background spectra for accurate absorbance calculations.

4.2 Sample preparation and Spectral acquisition

A gas-mixing station was constructed in order to prepare samples of methyl vinyl ketone for analysis. A valve system (Nupro Company, SS-4H-TH3) is connected to a vacuum pump (Varian, NW-25), a 1000 torr maximum pressure gauge (MKS instruments, 626C13TBE), a 250 mL glass bulb, a nitrogen tank, and a glass bubbler for sample introduction to the gas-mixing station. All connections were made with ultratorr fittings, Teflon tubing, and plastic tubing.

Methyl vinyl ketone was purchased from Alfa Aesar (90% purity). Several drops of the MVK was introduced to the bubbler and subjected to three rounds of freeze-pump-thaw cycles using liquid nitrogen to ensure sample purity. After purification, the system was evacuated and methyl vinyl ketone introduced to the system. The compound's inherent volatility facilitated this process as it readily vaporized, diffusing throughout the mixing station. The sample bulb was then attached to the multipass cell, introducing methyl vinyl ketone to the cell for the measurement of

spectra. When introducing the sample, <1.00 torr would be introduced in order to avoid the saturation of the spectra.

Pure MVK was introduced to the multipass cell and the pressure kept below 0.5 torr to avoid pressure broadening as well as saturation at the regions that absorbed intensely. Acquiring spectra at a low pressure is essential when acquiring high-resolution spectra as the linewidths of individual rotational lines are kept fairly small and can be resolved. Spectra of samples acquired at higher concentrations tend to have broad peaks that prevents the resolution of fine structure. A sweep-scan of MVK was acquired with the range of 970 – 1015 cm^{-1} in order to become familiar with the overall shape of the spectrum as well as a background over the same frequency range for the purpose of calculating the absorbance spectrum. Several dozen piezo scans and corresponding backgrounds were acquired across the target frequency range in order to construct the spectrum. Background spectra were acquired by evacuating the multipass cell and performing the acquisition under the same parameters of the corresponding sample spectra.

All MVK and background spectra were acquired in tandem with reference spectra of methanol in a direct absorption reference cell. The absorbance spectrum was then calculated for each acquisition of MVK. Absorbance was calculated using Equation 5 where Po is the incident light, obtained from the background, and P is the intensity of the transmitted light, obtained from the sample spectra. Frequency calibrations were performed on every methanol spectrum and the parameters of the calibrations applied to the corresponding MVK and background scans to calibrate them.

$$A = -log\frac{P}{P_o} \qquad (5)$$

4.3 Calibration methods

Acquired methanol spectra were compared with a reference methanol spectrum in the region of 970 – 1010 cm^{-1} that was generated by SpectraPlot[13] using spectral data found in the HITRAN[14] database. When generating the reference spectrum, the parameters were set to be similar to those of the spectrometer: P = 0.001 atm, T = 300 K, L = 50 cm. The step size for each point in the reference spectrum was set to 0.001 cm^{-1}. The necessitation for calibration can be noted by the discrepancy in frequency between the acquired methanol spectrum and the one generated by SpectraPlot using the HITRAN database in Figure 7.

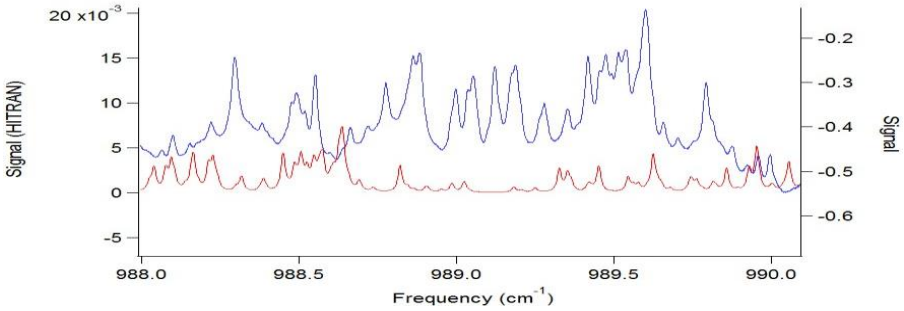

Figure 7: A methanol spectrum acquired using the piezo scanning method (blue) and a sample of the reference methanol spectrum (red) before the calibration was performed.

The point numbers for the peaks in all methanol spectra were matched with the frequencies of the corresponding peaks in the reference spectrum. The recorded point numbers and frequencies for each peak were treated as x and y values, respectively; then fitted to a 10^{th} order polynomial fit. The parameters for each methanol calibration were then applied to the MVK and background scans that were acquired in tandem to calibrate those as well. The calibrated spectra were then used to calculate absorbances with accurate frequency calibrations. All absorbance spectra were calculated using Equation 5.

4.4 Computational Chemistry

The optimized molecular structure for the *cis* conformer of MVK was calculated at the MP2/cc-pVTZ level of theory using the GAUSSIAN 16 software package.[21] Computational calculations were performed on the cis conformer as the work done by Lindenmeier and Durig confirmed that the trans-conformer did not exhibit any absorption in the target region.[5,7] Anharmonic vibrational frequencies as well as rotational constants for the ground and excited vibrational states were calculated with GAUSSIAN 16 following the structure optimization using second-order vibrational perturbation theory.[11] The calculated anharmonic vibrational frequencies for the ν_{22} and ν_{23} bands were then compared with the frequencies observed in the acquired spectrum, as well as the low-resolution spectra acquired by Lindenmeier et al.[5] The ground state rotational constants calculated using GAUSSIAN 16 were also compared with ground state rotational constants found experimentally by Wilcox et al.[22] The difference of the theoretical rotational constants was subtracted from the ground state experimental rotational constants that were found experimentally by Wilcox in order to determine a set of adjusted, excited state rotational constants. With the rotational constants of the ground and first-excited vibrational state, theoretical spectra for the regions of the ν_{22} and ν_{23} bands were simulated and subsequently compared to the observed spectrum.

5. Results and Discussion

5.1 High-resolution absorbance spectrum of MVK

The high-resolution spectrum of MVK from 970 – 1015 cm^{-1} is presented in Figure 8, and is overlayed with the background spectrum that was used to calculate the absorbance spectrum of MVK. Both spectra were acquired using the sweep-scan method. The consistent sinusoidal fluctuation across the sweep scan is the result of the laser's flux in power during spectral acquisition. These fluctuations do not pose an issue as they are consistent across the sweep and from scan to scan so that when calculating the absorbance spectrum, relative absorbances the features in the spectrum are unaffected. The spectrum of MVK demonstrated a shape typical of most ro-vibrational spectra, consisting of strong Q-branch regions with the P and R braches spreading out away from the Q-branches. The absorbance spectrum was then calculated from the sample spectrum and the background using Equation 5, and is displayed in Figure 9**.**

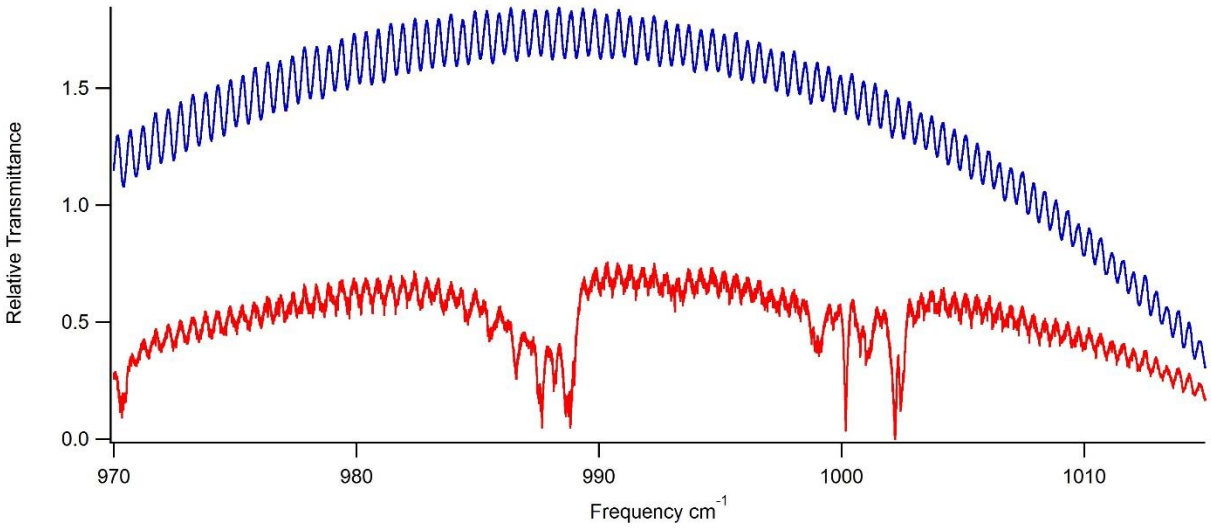

Figure 8: A sweep scan of a background (blue) and of methyl vinyl ketone acquired from 970 - 1010 cm^{-1}

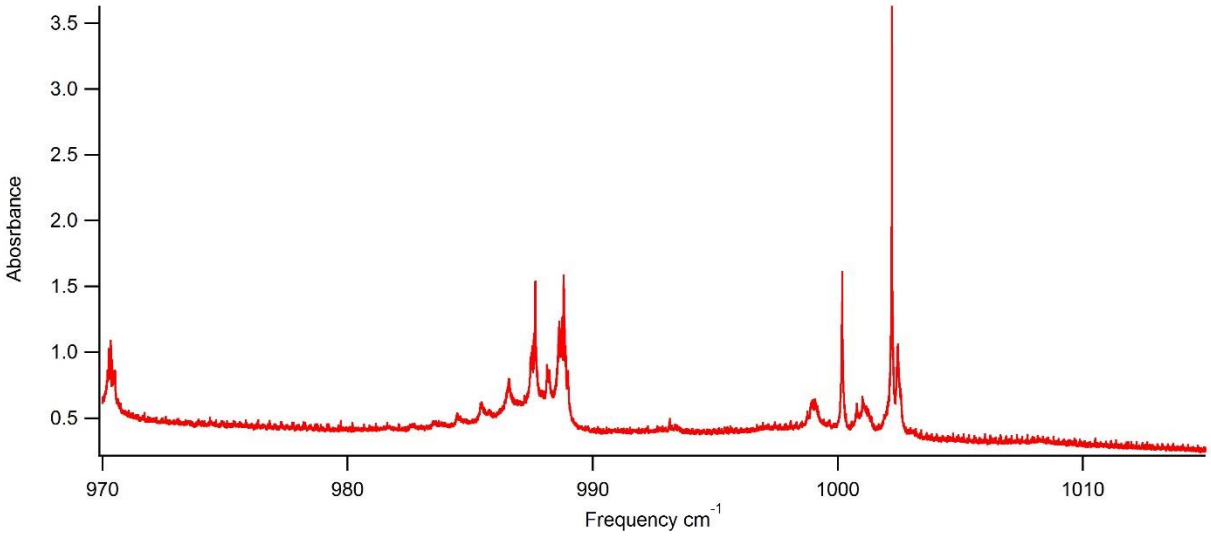

Figure 9: The high-resolution absorbance spectrum of methyl vinyl ketone acquired from 970 – 1015 cm-1 that was calculated from the spectra in Figure 8

The absorbance spectrum acquired with the sweep-scanning was able to further resolve the rotational structure as well as some additional vibrational bands in the spectrum of MVK. An expanded portion of the R branch of the ν_{23} transition is included in Figure 10 to demonstrate both the resolution of the rotationally resolved spectrum and its congestion. It is important to note that each peak visible in Figure 10 is the result of a rotational transition, not noise in the spectrum.

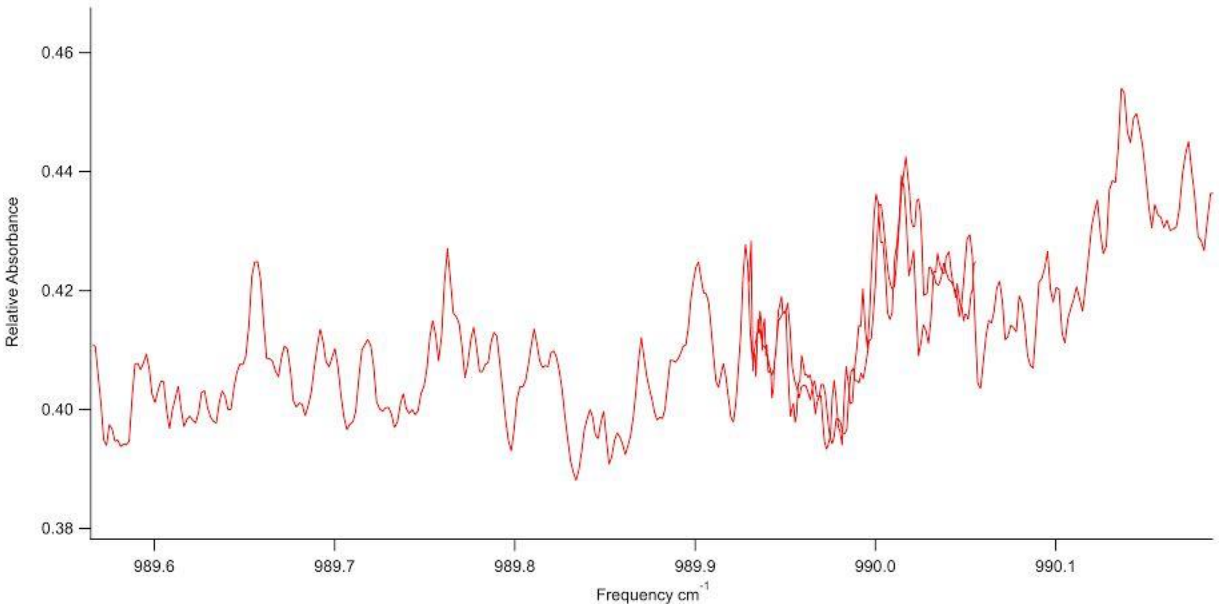

Figure 10: An expansion of the R branch from the ν_{23} vibrational band. This resolution is consistent across each piezo-scan and demonstrates the degree of congestion present in the rotational structure throughout the spectrum.

The spectrum's most notable features include many strong Q-branches surrounding the bands at 987.59 and 1001.031 cm^{-1} that were assigned to the ν_{23} and ν_{22} fundamental transitions, respectively, in previous studies of the IR spectrum of MVK.[5] The additional Q branch features that are red shifted from the fundamental transitions found at 986.44, 985.38, 984.31, and 998.98 cm^{-1} are believed to be the result of hot bands of ν_{23} and ν_{22}, respectively. Expansions of these two regions are presented in Figures 11 and 12, highlighting these additional bands.

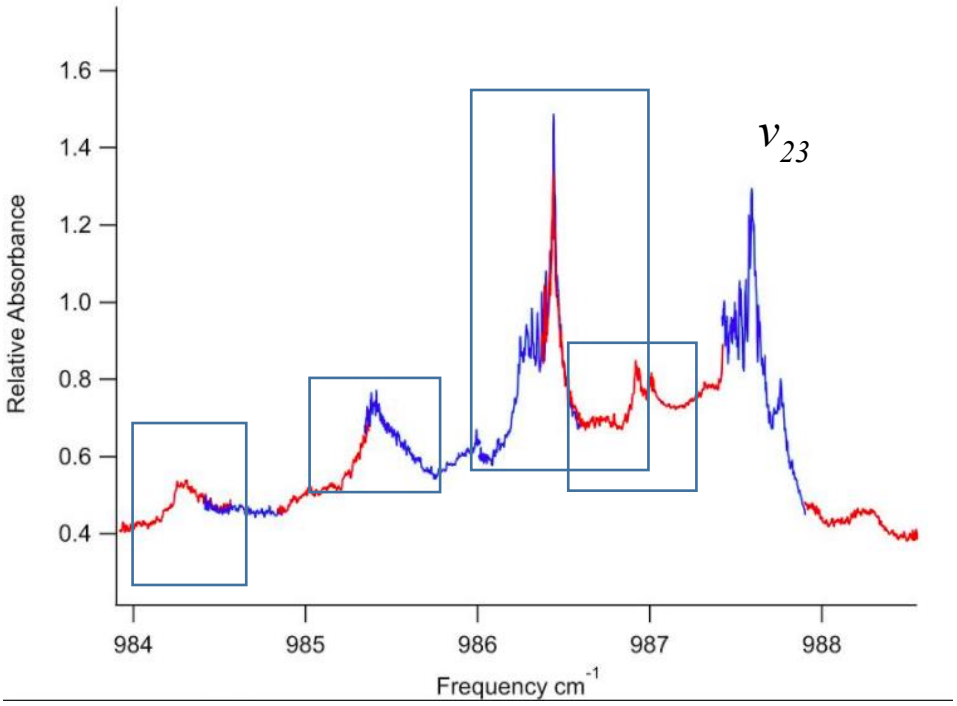

Figure 11: An expansion of the region containing the ν_{23} band that was acquired with the piezo scanning method. The additional Q-branch feature at 986.44, 985.38, and 984.31 cm^{-1} is enclosed by a box. The alternating blue and red color-scheme is used to differentiate between individual piezo scans.

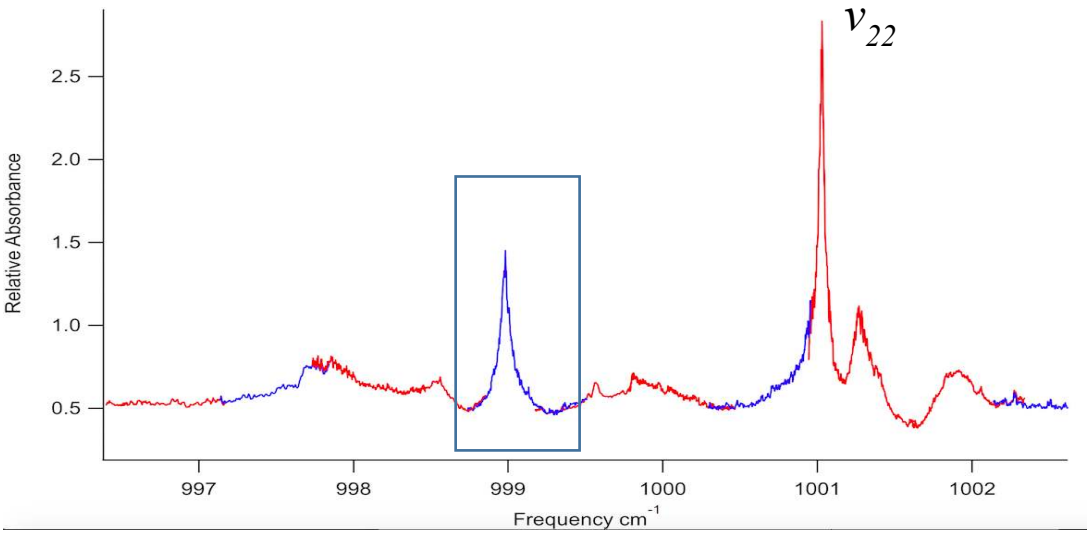

Figure 12: An expansion of the region of the high-resolution spectrum containing the ν_{22} band that was acquired with the piezo scanning method. The additional Q branch feature at 998.89 cm^{-1} are enclosed in boxes. The alternating blue and red color scheme is used to differentiate between individual piezo scans.

5.2 Calibration methods

The spectra included in the expansions, Figures 11 and 12, are comprised of several spectra acquired using the piezo scanning method, hence the alternating blue and red color-scheme that was implemented to differentiate between the consecutive acquisitions. Not only do these expansions demonstrate the resolved vibrational and rotational structure of MVK, they demonstrate the consistency of the applied frequency calibration methods. As the piezo scanning method is only able to acquire approximately 0.7 cm^{-1} for each acquisition, overlap becomes apparent as one spectrum continues on to the next. These overlapping regions of spectra were analyzed in order to determine the efficacy of the frequency calibration method. Although overlapping spectra are not completely superimposable, the deviation in peak frequency is very small across all overlapping spectra, with the smallest deviations being <0.001 cm^{-1}, and the largest no larger than ~0.003 cm^{-1}.

The slight variation in calibration accuracy is the result of several experimental factors, as well as those inherent to the method of calibration. The laser itself is a factor when it comes to the efficacy of the calibration. One variable that leads to uncertainty in the calibration comes from the piezo controller. When acquiring spectra with the piezo, the laser is scanning back and forth over the same frequency range for a given amount of time. This generates a repeating spectrum on a time axis that must be separated at the points of repetition. The repeated spectra are then averaged in order to improve the signal to noise ratio of the overall spectra, increasing the resolution. Although generally helpful, it is at the points of the turnaround where the laser acquires more points than throughout the rest of the scan, which leads to a small amount of additional noise in the spectrum. This becomes apparent in the tail-ends of the averaged piezo spectra. An example

of a piezo spectrum is presented in Figure 13 and the result of its segmentation and averaging in Figure 14.

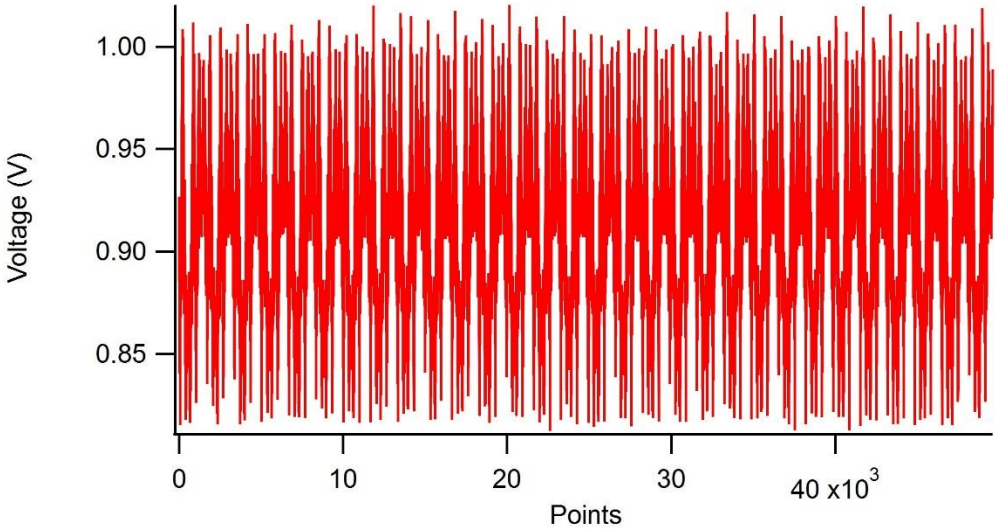

Figure 13: An acquired piezo spectrum prior to averaging of the repeating sections.

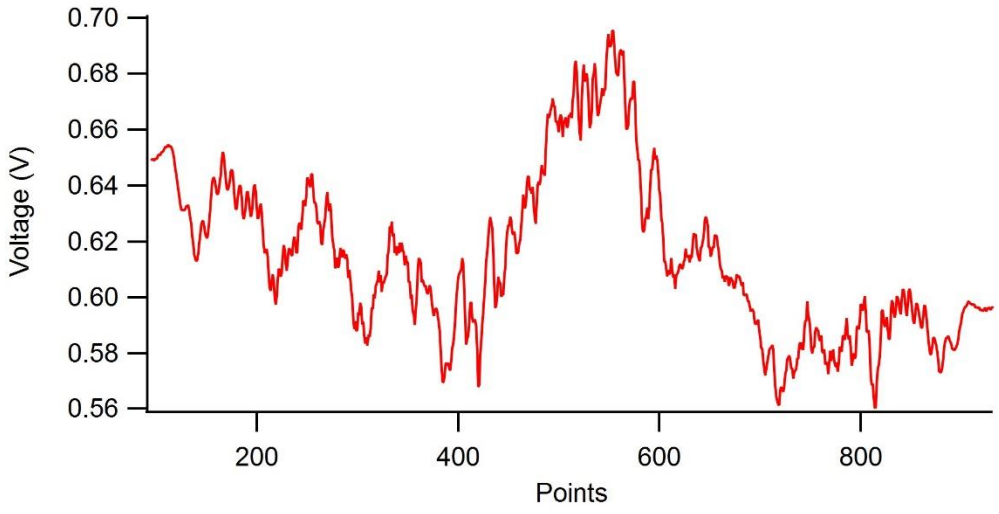

Figure 14: An averaged piezo spectrum of a sample of MVK at 974.75 cm^{-1}. What appears as slight decreases in resolution at the tail ends of this spectrum are actually the result of the laser spending more time at the frequencies near the turn-around.

Portions of various spectra that overlap during the turnaround region are also the ones that demonstrate the largest deviations once calibrated. For example, the two spectra that overlap in the R branch of the ν_{23} band in Figure 10 are at the turnaround areas, and have deviations of ~0.003 cm^{-1}. When calibrating the frequencies for each individual spectra, all of the experimental methanol peaks had to be matched with the corresponding peaks from the reference spectrum. The values of for each peak from the experimental and reference spectra were treated as x and y values, respectively and subjected to a 10^{th} order polynomial fit. Since the number of methanol peaks were the values used to generate the polynomial, the frequency ranges that included more methanol peaks were able to generate more agreeable fits when calibrated as the polynomial could be generated more accurately to match the data. One final source for uncertainty in the calibration comes from the difficulty of acquiring spectra at reliably consistent pressures. Although the pressure was kept as consistent as possible for each new sample, very slight leaks in the system, particularly the methanol reference cell, would lead to different degrees of pressure broadening in the sample spectra, as well as methanol spectra. The leaks proved to be the most problematic with regards to the reference cell as rotational lines would begin to blend together due to pressure broadening. Pressure broadening would effectively decrease the number of observable lines that could be used for the calibration. The reference cell was refreshed frequently enough that this was, overall, not a major contributor to calibration issues.

Ultimately, the spectra acquired using the piezo scanning method were calibrated and stitched together in order to construct the MVK spectrum within the target range of 980 – 1010 cm^{-1}, as seen in Figure 15. It was also necessary to scale the relative intensities of each individual piezo scan due to how the pressure in the multipass cell was inconsistent between scans. Scaling was accomplished by adjusting the relative intensities of adjacent piezo scans to reflect the

differences of the relative absorbance of the same regions that were observed using the sweep scanning method.

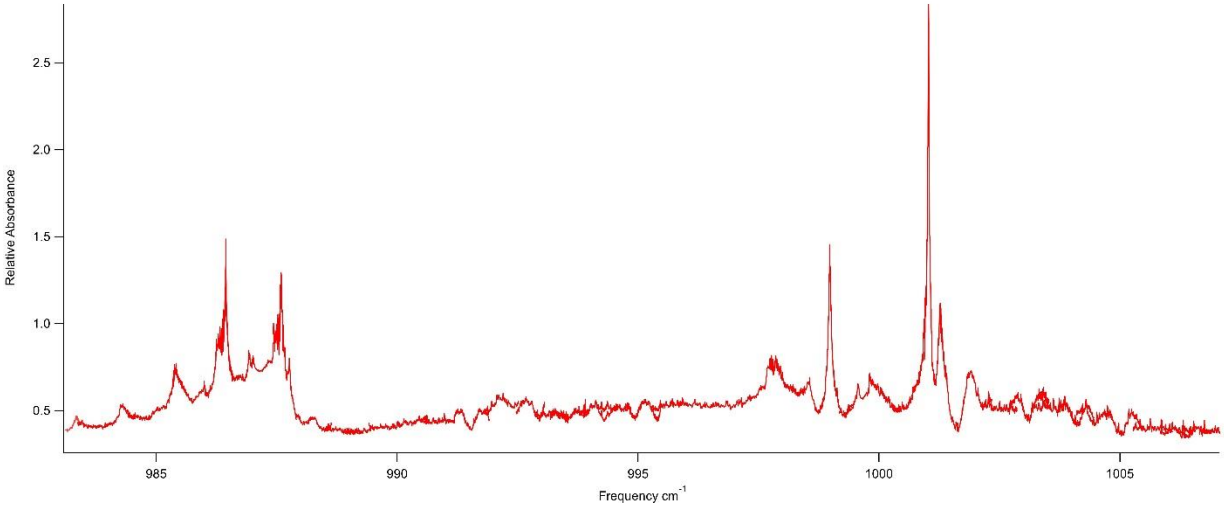

Figure 15: The Calibrated high-resolution absorbance spectrum of MVK from 980 – 1010 cm^{-1} comprised of individual spectra acquired using the piezo-scanning method.

5.3 Computational Chemistry & Simulations

The molecular geometry of for both the *cis* and *trans* conformers of MVK were calculated at the MP2 level of theory with cc-pVTZ basis sets using the software Gaussian 16. The anharmonic vibrational frequencies for the 27 vibrational modes, see Equation 1, were also calculated for both conformers. Table 2 includes the assignments for the cis-conformer, as our calculations indicate that no fundamental transitions of trans-MVK are visible within the target region. This statement is confirmed by previous calculations and experimental data performed by Durig and Lindenmaier et al.[5,7]

Table 2: Vibrational assignments for cis-MVK. Computational and experimental assignments are included from PNNL for comparison.[5]

Mode	Observed Frequency (cm^{-1})	Observed (PNNL) Frequency (cm^{-1})	Calculated MP2/cc-pVTZ (This work) Frequency (cm^{-1})	Calculated PQS SQM (PNNL) Frequency (cm^{-1})
ν_1		3109.098	3086	3122
ν_2		3060.68	3152	3044
ν_3		3040.72	3064	3034
ν_4		3019.51	3078	3031
ν_{19}		2968.86	3016	2967
ν_5		2934.56	2967	2914
ν_6		1735.30	1726	1731
ν_7		1622.56	1632	1624
ν_{20}		1442.92	1451	1443
ν_8		1428.66	1433	1434
ν_{19}		1399.81	1404	1395
ν_{10}		1357.81	1351	1353
ν_{11}		1298.14	1297	1296
ν_{12}		1180.59	1186	1178
ν_{13}		1064.28	1061	1062
ν_{21}		1042.44	1028	1029
ν_{22}	1001.0309	1001.12	1003	1008
ν_{23}	987.5917	987.58	975	975

v_{14}		952.36	953	939
v_{15}		773.50	776	757
v_{24}		664.41	669	671
v_{16}		598.43	598	594
v_{25}		N/O	450	456
v_{17}		413.38	413	413
v_{18}		270.04	272	270
v_{26}		109.35	173	126
v_{27}		86.90	44	107

The fundamental v_{23} and v_{22} transitions demonstrate Q-branch structure that is generally associated with the C-type bands of excited asymmetric tops. Included in Figure 16 are the force vectors for these specific vibrations. The v_{23} vibrational motion is best described as an out of phase bend of the terminal $C{=}CH_2$ while the v_{22} vibrational motion is best described as an out of phase bend of the -C**H**=C. Bands akin to the v_{23} and v_{22} transitions are often ideal targets for acquiring spectroscopic data on atmospheric samples using IR spectroscopy due to the intensity of absorption inherent to the band type. For example, previous experiments involving acquiring spectra of isoprene have specifically targeted the v_{26} C-type vibrational band near 992 cm^{-1}.

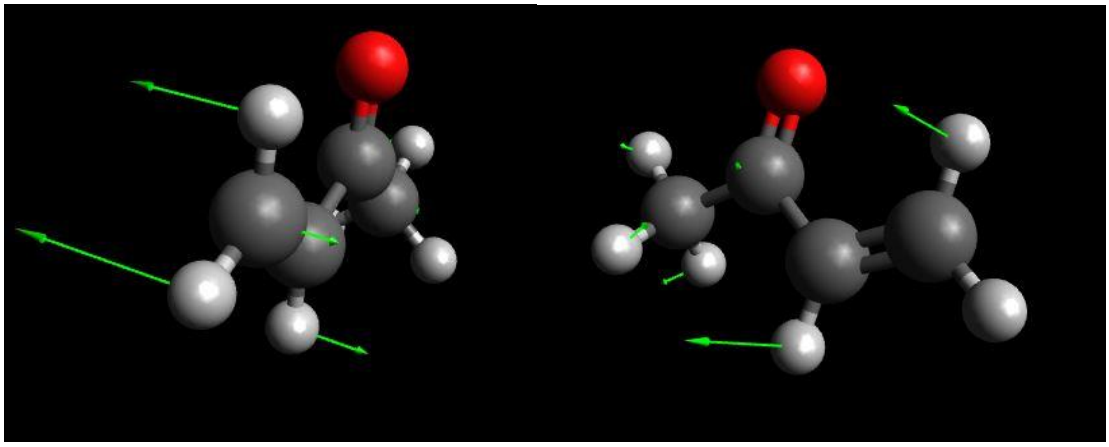

Figure 16: Force vector models of cis-MVK for the v_{23} transition (left) and v_{22} transition (right) demonstrating their respective vibrational motions

Although the fundamental transitions have been assigned, previous work has not begun to suggest assignments of the additional Q-branch structures. The high-resolution spectrum resolves additional, non-fundamental vibrational transitions red-shifted to the v_{23} band at 986.44, 985.38, and 984.31 cm^{-1}; as well as one red-shifted to the v_{22} band at 998.98. It is postulated that the majority of these additional bands are the result of hot bands of v_{23} and v_{22} vibrations originating from several low-lying modes of MVK. Hot bands are the result of transitions from the excitation of a lower lying vibrational band to another as the result of heat. Hot bands appear as bands that are red-shifted to the fundamental vibrational band belonging to the mode that they were excited into. Assignments of the original low-lying modes of hot bands can be made by comparing the relative intensity of said hot bands to the relative intensity of their neighboring fundamental transition bands. The ratio of the intensity of the hot band to the fundamental band is given by the Boltzmann distribution given by Equation 6, where K_b is the Boltzmann constant, T is the temperature in kelvin, v is the frequency of the lower lying vibrational mode, N is the population of the hot band, and N_o is the population of the fundamental vibrational mode. The ratio of the populations is representative of the ratio of the intensity of the two bands.

$$\frac{N}{N_o} = e^{\frac{-v}{K_b T}} \qquad (6)$$

This equation was used to assign a hot band originating from the v_{26} mode; a hot band from this mode is expected to exhibit an absorbance that is 59% the intensity of the fundamental transition for the mode that it now populates. When comparing the relative absorbance of the peak assigned to the v_{22} band and the peak at 998.98 cm^{-1}, it is found that the latter does have an intensity that is approximately 59% of the fundamental transition. The Boltzmann distribution was also calculated for the following low-lying vibrational modes: v_{27}, v_{18}, and v_{17}. The results of this calculation suggest that hot bands that arise from these modes would exhibit relative intensities of 0.66, 0.27, and 0.13, respectively, when compared to the fundamental transition band of the mode they now populate.

The rotational constants for both the ground state and first excited state of cis-MVK were also calculated using second order perturbation theory (MP2) with a ccp-VTZ basis set. These rotational constants as well as the ground state rotational constants observed by Wilcox et al, were used to begin a simulation of the region containing the v_{23} and v_{22} transitions.[22] It was assumed that the differences between the calculated ground and excited state constants would be comparable to that of those observed experimentally. Thus, this difference between the calculated constants was applied to the constants observed by Wilcox et al in order to establish a set of adjusted constants representative of the first excited vibrational state. This methodology was adapted from the approach used by Sadiek and Friedrichs.[23] The Calculated, observed, and adjusted sets of rotational constants are recorded in Table 3.

Table 3 Calculated and observed rotational constants for MVK at the ground and excited states

Rotational Constants	Calculated MP2/cc-pVTZ *v = 0*	Observed *v = 0*	Calculated MP2/cc-pVTZ *v = 1*	Adjusted *v = 1*
A	0.338702	0.3416009	0.337910	0.3408089
B	0.133267	0.1331466	0.133112	0.1329916
C	0.097409	0.09758911	0.097387	0.09756711

Preliminary simulations for the IR spectrum of cis-MVK were performed using PGOHPER[24]. The observed ground state and adjusted excited state rotational constants were used as a starting point for the simulation. While editing the simulation, the observed ground state rotational constants were fixed and changes were only made to the adjusted constants. The initial simulations for the v_{23} and v_{22} modes can be seen in Figures 17 and 18**.**

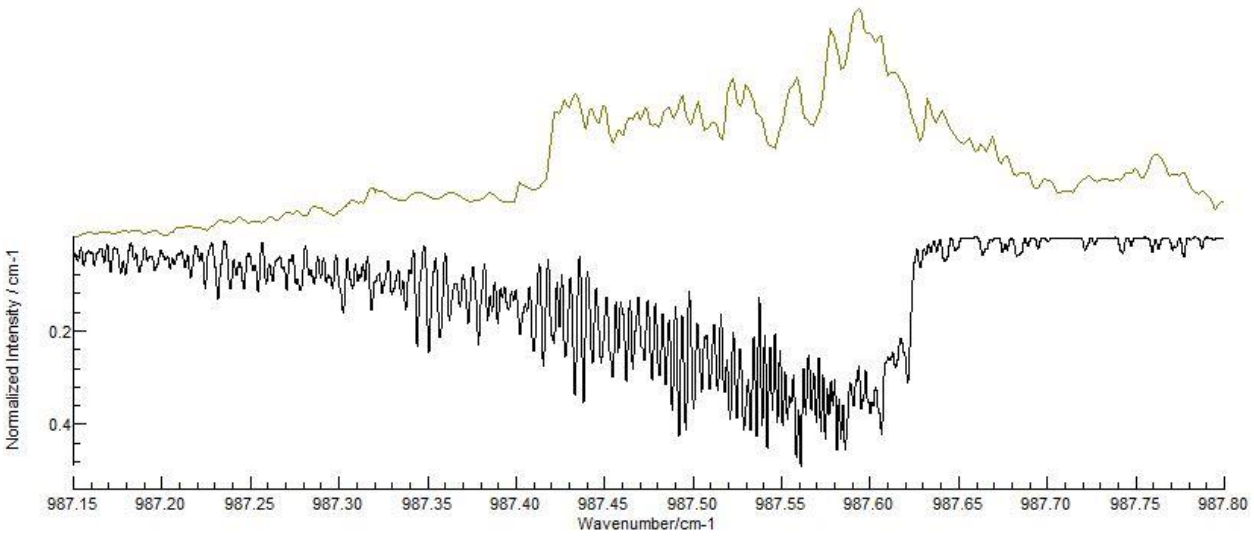

Figure 17: Simulation of the v_{23} vibrational band (black) generated with the observed ground state and adjusted excited state rotational constants compared to the high-resolution spectrum of the same region (green).

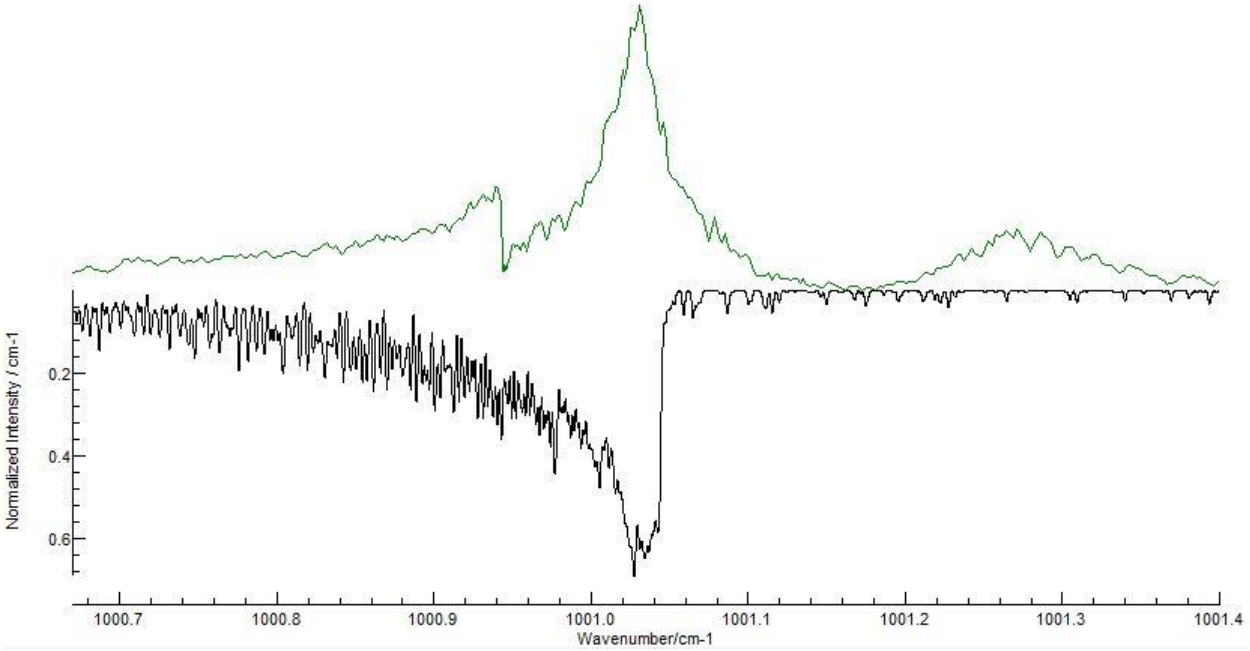

Figure 18*:* Simulation of the v_{22} vibrational band (black) generated with the observed ground state and adjusted excited state rotational constants compared to the high-resolution spectrum of the same region (green).

The simulations for the observed fundamental transitions were calculated at a rotational temperature of 300 K with linewidths of 0.0018 cm^{-1}. The molecule was said to belong to the C_s symmetry point group, and the v_{23} and v_{22} bands were both simulated as C-type. The preliminary simulations do match the general shape of their respective bands, but continued work with the simulations will be performed to improve upon their accuracy. When editing the rotational constants, it quickly became apparent that changing the constant C had the largest effects on the simulation, completely altering the shape unless changes were made on the order of $1x10^{-6}$ cm^{-1}, while finer structural changes could be performed with the other two constants. A detailed rotational analysis of the P and R-branch regions of the v_{23} and v_{22} has not been attempted due to the highly congested rotational structure present in these regions. Future studies may include performing high-resolution spectroscopy on cis-MVK at a much colder temperature. By acquiring

high resolution spectra of a cooled sample, the simplified rotational structure and absence of hot bands would help to confirm the current vibrational assignments, and also suggest whether or not the additional, unassigned Q-branches are the result of combination bands or fermi resonances.

6. Conclusions

The first high-resolution infrared spectrum of methyl vinyl ketone has been acquired in the region of the ν_{23} and ν_{22} bands from 970 – 1015 cm^{-1}. A frequency calibration was also performed on individual piezo spectra in order to establish accurate frequencies for the high-resolution spectrum. The high-resolution spectrum clearly resolves several Q-branches that are the result of non-fundamental transitions in this region, leading to the assignment of the Q-branch at 998.89 cm^{-1} as a hot-band of ν_{23} that arose from the ν_{26} mode. Anharmonic calculations completed at the MP2/cc-pVTZ level of theory were completed to determine the molecular geometry of cis-MVK, assist with vibrational assignments, and to calculate the ground and excited state rotational constants. The rotational constants were used to begin simulating the theoretical spectrum of cis-MVK. This work will prove useful when continuing to assign the additional Q-branch features noted in this region, and for future studies that involve performing atmospheric measurements of MVK.

7 References

(1) Guenther, A.; Karl, T.; Harley, P.; Wiedinmyer, C.; Palmer, P. I.; Geron, C. Estimates of Global Terrestrial Isoprene Emissions Using MEGAN (Model of Emissions of Gases and Aerosols from Nature). *Atmos. Chem. Phys.* **2006**, *6* (11), 3181–3210.

(2) Atkinson, R.; Arey, J. Gas-Phase Tropospheric Chemistry of Biogenic Volatile Organic Compounds: A Review. In *Atmospheric Environment*; 2003; Vol. 37.

(3) Claeys, M.; Graham, B.; Vas, G.; Wang, W.; Vermeylen, R.; Pashynska, V.; Cafmeyer, J.; Guyon, P.; Andreae, M. O.; Artaxo, P.; et al. Formation of Secondary Organic Aerosols through Photooxidation of Isoprene. *Science* **2004**, *303* (5661), 1173–1176.

(4) Karl, M.; Brauers, T.; Dorn, H.-P.; Holland, F.; Komenda, M.; Poppe, D.; Rohrer, F.; Rupp, L.; Schaub, A.; Wahner, A. Kinetic Study of the OH-Isoprene and O_3 -Isoprene Reaction in the Atmosphere Simulation Chamber, SAPHIR. *Geophys. Res. Lett.* **2004**, *31* (5)

(5) Lindenmaier, R.; Williams, S. D.; Sams, R. L.; Johnson, T. J. Quantitative Infrared Absorption Spectra and Vibrational Assignments of Crotonaldehyde and Methyl Vinyl Ketone Using Gas-Phase Mid-Infrared, Far-Infrared, and Liquid Raman Spectra: S-Cis vs S-Trans Composition Confirmed via Temperature Studies and Ab Init. *J. Phys. Chem. A* **2017**, *121* (6), 1195–1212.

(6) Foster, P. D.; Rao, V. M.; Curl, R. F. Microwave Spectrum of Methyl Vinyl Ketone. *J. Chem. Phys.* **1965**, *43* (3), 1064–1066.

(7) Durig, J. R.; Little, T. S. Conformational Barriers to Internal Rotation and Vibrational Assignment of Methyl Vinyl Ketone. *J. Chem. Phys.* **1981**, *75* (8), 3660–3668.

(8) Iannone, R.; Koppmann, R.; Rudolph, J. 12C/13C Kinetic Isotope Effects of the Gas-

Phase Reactions of Isoprene, Methacrolein, and Methyl Vinyl Ketone with OH Radicals. *Atmos. Environ.* **2009**, *43* (19), 3103–3110.

(9) Yokelson, R. J.; Christian, T. J.; Karl, T. G.; Guenther, A. The Tropical Forest and Fire Emissions Experiment: Laboratory Fire Measurements and Synthesis of Campaign Data. *Atmos. Chem. Phys.* **2008**, *8* (13), 3509–3527.

(10) Barone, V. Anharmonic Vibrational Properties by a Fully Automated Second-Order Perturbative Approach. *J. Chem. Phys.* **2005**, *122* (1).

(11) McQuarrie, D. A.; Simon, J. D. *Physical Chemistry: A Molecular Approach*; 1997.

(12) Hollas, J. M. Modern Spectroscopy, 4th Edition. *J. Chem. Educ.* **2005**, *82*, 43.

(13) Goldenstein, C. S.; Miller, V. A.; Mitchell Spearrin, R.; Strand, C. L. SpectraPlot.com: Integrated Spectroscopic Modeling of Atomic and Molecular Gases. *J. Quant. Spectrosc. Radiat. Transf.* **2017**, *200*, 249–257.

(14) Rothman, L. S.; Gordon, I. E.; Barbe, A.; Benner, D. C.; Bernath, P. F.; Birk, M.; Boudon, V.; Brown, L. R.; Campargue, A.; Champion, J. P.; et al. The HITRAN 2008 Molecular Spectroscopic Database. *J. Quant. Spectrosc. Radiat. Transf.* **2009**, *110* (9–10), 533–572.

(15) Faist, J.; Capasso, F.; Sivco, D. L.; Sirtori, C.; Hutchinson, A. L.; Cho, A. Y. Quantum Cascade Laser. *Science (80-.).* **1994**, *264* (22), 553–556.

(16) Kazarinov, R. F.; Suris, R. A. Possibility of the Amplification of Electromagnetic Waves in a Semiconductor with a Superlattice. *Sov. Phys. - Semicond.* **1971**, *5* (4), 707–709.

(17) Cascade_transitions @ Upload.wikimedia.org.

(18) Hannemann, M.; Antufjew, A.; Borgmann, K.; Hempel, F.; Ittermann, T.; Welzel, S.; Weltmann, K. D.; Völzke, H.; Röpcke, J. Influence of Age and Sex in Exhaled Breath Samples Investigated by Means of Infrared Laser Absorption Spectroscopy. *J. Breath Res.*

2011, *5* (2).

(19) Duxbury, G.; Langford, N.; McCulloch, M. T.; Wright, S. Quantum Cascade Semiconductor Infrared and Far-Infrared Lasers: From Trace Gas Sensing to Non-Linear Optics. *Chem. Soc. Rev.* **2005**, *34* (11), 921.

(20) Pereira, Marcus; Hoadley, Tyler; Iranpour, Michael; Tran, Minh; Stewart, J. *High Resolution Infrared Spectroscopy of the v26 Band of Isoprene*; 2018.

(21) Frisch, M. J. G.; Trucks, W.; Schlegel, H. B.; Scuseria, G. E.; Robb, M. A.; Cheeseman, J. R.; Scalmani, G.; Barone, V.; Mennucci, B.; Petersson, G. A.; et al. *Gaussian 16, Rev. A.03*; 2016.

(22) Wilcox, D. S.; Shirar, A. J.; Williams, O. L.; Dian, B. C. Additional Conformer Observed in the Microwave Spectrum of Methyl Vinyl Ketone. *Chem. Phys. Lett.* **2011**, *508* (1–3), 10–16.

(23) Sadiek, I.; Friedrichs, G. Doppler-Limited High-Resolution Spectrum and VPT2 Assisted Assignment of the C-H Stretch of CH2Br2. *Spectrochim. Acta - Part A Mol. Biomol. Spectrosc.* **2017**, *181*, 180–191.

(24) Western, C. M. PGOPHER: A Program for Simulating Rotational, Vibrational and Electronic Spectra. *J. Quant. Spectrosc. Radiat. Transf.* **2017**, *186*, 221–242.